Structural effects of pressure on triclinic chlorite: A single-crystal study

P.F. Zanazzi,* M. Montagnoli, S. Nazzareni, and P. Comodi

Dipartimento di Scienze della Terra, Università di Perugia, Piazza Università, I-06100 Perugia, Italy

Abstract

We present the results of a single-crystal X-ray diffraction structural study of chlorite in a diamond anvil cell up to 5.47 GPa. The sample is a clinochlore from Val Malenco, Italy, triclinic polytype IIb-4, S.G. $C\bar{1}$, with pseudomonoclinic metric and composition $(Mg_{9.14}Fe^{2+}_{1.02}Fe^{3+}_{0.01} Mn_{0.01}Ti_{0.01}Al_{1.76})_{\Sigma=11.95}(Si_{6.32} Al_{1.68})_{\Sigma=8}O_{20}(OH)_{16}$. Structural refinements were performed at several pressures with intensity data collected on a CCD diffractometer. Unit-cell parameters were accurately measured with the point-detector mounted on the same instrument.

The bulk modulus of chlorite fitting data to a third-order Birch-Murnaghan equation of state is $K_0. = 88(5)$ GPa with $K' = 5(3)$. Results are in fair agreement with data based on powder neutron and synchrotron diffraction methods. The axial compressibility values were $\beta^{EoS}_{0a} = 3.4(2)$, $\beta^{EoS}_{0b} = 3.4(1)$, and $\beta^{EoS}_{0c} = 5.4(2)$ 10^{-3} GPa^{-1}. The metric of the lattice remains triclinic in the investigated pressure range. Axial anisotropy is strongly reduced with respect to the axial compressibilities observed in other phyllosilicates. Comparison of structural refinements at different pressures shows that the main structural deformations affect the interlayer region, where the hydrogen bonds are relevant to the structural properties of the phase. The mean decrease of the OH-O distances is about 10% from ambient pressure to ~5 GPa.

Compressibility data may be combined with those on thermal expansion to formulate an equation of state for clinochlore. Taking into account the thermal expansion coefficient reported in literature for a chlorite with a composition quite similar to that of our sample, we can write the equation: $V = V_0 (1 - 1.14 \ 10^{-2} \ \Delta P + 2.316 \ 10^{-5} \ \Delta T)$, where P is in GPa and T in Celsius. Assuming an average rock density of 2.7 g/cm^3, this corresponds to an isochoric P-T geothermal gradient of 18 °C/km.

Keywords: Chlorite, compressibility, equation of state, high pressure

Introduction

In the recent years, many authors have been interested in the stability range and decomposition of chlorite, because this mineral is among the hydrous phases having a role in the upper mantle mass transport and melting processes. Provided enough aluminum is present in descending material (such as the pelitic oceanic sediment), H_2O can be stored in hydrous minerals as lawsonite, staurolite, epidote, and chlorite (Poli and Schmidt 2002), other than in serpentine (Ulmer and Trommsdorff 1995). As a consequence, the breakdown of these phases will determine the actual dehydration of the slab. Chlorite contains around 13 wt% of water and also in a limited amount could strongly influence the slab buoyancy. There are few experimental studies on the stability conditions of chlorite. The most thermally stable chlorite composition is clinochlore, nominally $Mg_5Al_2Si_3O_{10}(OH)_8$, but many compositions show both Tschermak's and Fe-Mg substitution.

Recently, petrological experiments (Fumagalli and Poli 2005) in the Na_2O-CaO-FeO-MgO-Al_2O_3-SiO_2-H_2O (NCFMASH) found that the presence of Fe shifts the thermal stability of chlorite toward lower temperatures, as compared with phase equilibria in the simpler system MASH. Pawley (2003) has recently bracketed the reaction clinochlore + enstatite = forsterite + pyrope + H_2O up to 5 GPa. At P/T higher than 4.8 GPa and 680 °C, an Al-bearing 10 Å phase was found to grow at the expense of chlorite (Fumagalli and Poli 2005), defining a new reaction leading to the disappearance of chlorite. As a consequence, the reaction involving chlorite and 10 Å phase should represent a critical step in the generation of fluids relevant for arc-magmatism.

Chlorite is a widespread family of di- and trioctahedral layer silicates. The trioctahedral chlorite structure can be described as formed by double layers of talc-type, negatively charged 2:1 layers, with ideal composition $(R^{2+},R^{3+})_3(Si_{4-x}Al_x)O_{10}(OH)_2$ separated by interlayer brucite-type octahedral layers [positively charged, with composition $(R^{2+},R^{3+})_3(OH)_6$; Bailey 1988]. The electrostatic interactions and a system of hydrogen bonding between T-O-T layer and O-interlayer contribute to the stability of the structure. Different T-O-T and O layer sequences are possible, creating a large number of different polytypes (Bailey 1988). The triclinic IIb-4 polytype, with symmetry $C\bar{1}$, and the monoclinic IIb-2 polytype, with symmetry $C2/m$ are the most abundant regular stacking one-layer chlorites occurring in nature. The triclinic structure was refined and described by several authors (X-ray diffraction: Steinfink 1958; Phillips et al. 1980; Zheng and Bailey 1989; Joswig and Fuess 1990; Neutron diffraction: Joswig et al. 1980). The monoclinic structure was

* E-mail: zanazzi@unipg.it

described by Zheng and Bailey (1989), Rule and Bailey (1987), and Joswig and Fuess (1989).

In view of chlorite being a major carrier of water in subducting slabs, it is important to know the stability field of this hydrous phase by studying its compressibility and pressure dependence of its crystal structure. Hazen and Finger (1978) based on only two data points at pressure carried out a pioneering single-crystal study on the behavior of chlorite up to 4 GPa, but the reliability of their results was hindered by the poor quality of the sample. To date, no other high-pressure single-crystal study has been reported, likely owing to the difficulty in finding suitable samples. Chlorite natural crystals are normally affected by stacking disorder and intergrowths, which make difficult to obtain reliable results. Welch and Marshall (2001) performed neutron high-pressure powder diffraction experiments on synthetic monoclinic clinochlore. Welch and Crichton (2002) determined the compressibility of synthetic II*b* clinochlore (metrically monoclinic) up to 8 GPa with synchrotron powder data. Kleppe et al. (2003) studied the effect of pressure on the hydrogen bonding system of chlorite with Raman spectroscopy up to 26.5 GPa. On the basis of the abrupt change in the frequency of the OH involved in hydrogen bonds, these authors claim that a "non quenchable," reversible transformation occurs between 9 and 10 GPa. Recently synchrotron powder diffraction patterns up to 27 GPa were reported by Welch et al. (2004) showing that the transformation is isosymmetric ($C\bar{1}$) and has a small change in β monoclinic angle from 97.2 to 96.3°, probably due to a rearrangement of the interlayer hydrogen-bond system.

The effect of chemical substitution on the baric behavior of chlorite was also investigated by different authors but the results are not entirely consistent. Pawley et al. (2002) reported the compressibility of three chlorite compositions based on synchrotron energy-dispersive powder data and found a similar compressibility for all three compositions. On the other hand, Theye et al. (2003) analyzed the effect of Fe-Mg substitution on the compressibility of chlorite by using a multi anvil press and synchrotron EDS data. They found that the compressibility of a synthetic chamosite is higher, and that of a natural chamosite lower, than that of clinochlore. The difference was tentatively explained by the presence of crystal defects.

The aim of the present work on good quality single crystals is to define an equation of state for a natural triclinic II*b*-4 chlorite and to investigate the nature of the deformation induced by pressure on the atomic arrangement, with special attention to changes in the hydrogen-bonded interlayer region.

EXPERIMENTAL METHODS

A natural II*b*-4 chlorite from Alpe Reguzzolo, Val Malenco (Italy), kindly supplied by the Mineralogy Museum of Florence University (no. 13087/626), was selected for high-pressure X-ray diffraction experiments. The samples are green platy crystals; their chemical composition was determined using an electron microprobe Cameca SX50 (IGG-section of Padova) by averaging seven spot analyses to obtain the formula:

$(Mg_{9.14}Fe^{2+}_{1.02}Fe^{3+}_{0.01}Mn_{0.01}Ti_{0.01}Al_{1.76})_{\Sigma=11.95}(Si_{6.32}Al_{1.68})_{\Sigma=8}O_{20}(OH)_{16}.$

This composition corresponds to a clinochlore, following the terminology of Bayliss (1975).

For the refinement at room conditions, a triclinic crystal ($0.12 \times 0.08 \times 0.01$ mm in size) was mounted on a XCALIBUR (Oxford Diffr.) diffractometer equipped

with both CCD area and point detectors, operating at 50 kV and 40 mA, and using graphite monochromated Mo radiation ($\lambda K\alpha_1 = 0.7093$ Å). Diffraction data were first collected at room conditions with the area detector from the crystal in air. To maximize the reciprocal space coverage, a combination of ω and φ scans was used, with a step size of 0.4° and a time of 30 s/frame for a total of 1800 frames. Data were corrected for absorption with the program SADABS (Sheldrick 1996). Details of data collection and refinement are reported in Table 1. The unit-cell parameters were accurately measured by using the point detector and calculated by the least-squares fit of Bragg angles for about forty selected reflections in the θ range 5–25° and are reported in Table 2. The calculated density, assuming $Z = 1$, is $d_{calc} = 2.70$ g/cm³. The crystal structure refinement was carried out with anisotropic displacement parameters using the SHELX-97 program (Sheldrick 1997), starting from the atomic coordinates of Joswig and Fuess (1990). Neutral atomic scattering factors and $\Delta f'$, $\Delta f''$ coefficients from International Tables for Crystallography (Wilson and Prince 1999) were used. Full occupancy was assumed for all cation sites. The electronic density in the octahedral cation sites was accounted for by fitting the scattering factor curves of Mg and Fe with variable occupancy, and that of tetrahedral sites with the curves of Si and Al. The resulting sum of electrons in the cell was 157.2 and 109.3 e⁻ for octahedral and tetrahedral sites, in good agreement with data calculated on the basis of the chemical analysis (159.8 and 110.3 e⁻, respectively). The hydrogen atoms were localized in the difference electronic density map and included in the last cycles of refinement with equal isotropic atomic displacement factors and constraining the bond distance from the oxygen to 0.85 ± 0.05 Å. Their positions are reasonably close to those from neutron data refinement of Joswig et al. (1980). At the end of the refinement, no peak larger than 0.9 e⁻/Å³ was present in the final difference Fourier synthesis. Table 3[1] lists the observed and calculated structure factors. The atomic coordinates are listed in Table 4.

HIGH-PRESSURE EXPERIMENTS

For the high-pressure crystal-structure refinements, a chlorite sample (sample 1) with a chip of Sm²⁺:BaFCl and a fragment of α-quartz, was mounted in a Merrill-Bassett diamond anvil cell (DAC), equipped with type-I diamonds with 800 μm culet face diameter. The pressure chamber was a 380 μm diameter hole, made by spark erosion on a 250 μm thick steel Inconel 750X gasket preindented to 180 μm. A methanol-ethanol mixture (4:1) was used as hydrostatic pressure-transmitting medium. The wavelength shift of the 6876 Å Sm²⁺ fluorescence line was measured

TABLE 1. Details of data collection and refinement at various pressures

P (GPa)	0.0001*	1.83	3.14	4.25	4.85
θ–range	3–35°	3–30°	3–30°	3–30°	3–30°
crystal-detector distance (mm)	65	65	65	65	65
No. measured reflections	4592	3758	3997	1122	1859
No. independent reflections	2135	484	478	208	351
Reflections with *l* > 4σ(*l*)	1728	424	397	175	291
No. refined parameters	156	56	56	56	56
R_{int}%	1.3	7.7	8.7	4.4	5.6
R_1%	2.3	5.4	5.3	3.3	5.5

* Data collected with the sample in air.

TABLE 2. Unit-cell parameters at different pressures

P (GPa)	*a* (Å)	*b* (Å)	*c* (Å)	α (°)	β (°)	γ (°)	*V* (Å³)
mounting I							
1E-4	5.327(4)	9.233(6)	14.381(6)	90.2(2)	97.2(2)	89.97(6)	701.72(6)
0.81	5.317(1)	9.214(1)	14.333(6)	90.12(3)	97.20(6)	89.97(2)	696.5(1)
1.65	5.3030(7)	9.189(1)	14.270(5)	90.09(3)	97.20(3)	89.96(1)	689.9(2)
2.62	5.288(1)	9.164(1)	14.203(6)	90.16(3)	97.17(5)	89.98(2)	682.9(1)
3.24	5.277(1)	9.141(2)	14.163(5)	90.11(4)	97.22(4)	89.97(2)	677.8(1)
4.25	5.2618(01)	9.114(1)	14.106(5)	90.12(3)	97.20(3)	89.97(1)	671.1(1)
4.85	5.252(3)	9.106(5)	14.11(3)	90.1(1)	97.3(1)	89.93(5)	669.3(5)
5.47	5.24(1)	9.11(2)	14.06(5)	90.0(3)	97.5(3)	89.9(2)	665.6(6)
mounting II							
0.4	5.329(3)	9.222(4)	14.36(1)	90.30(6)	97.17(6)	89.95(4)	699.9(3)
1.2	5.307(4)	9.201(5)	14.28(2)	90.22(8)	97.14(8)	89.95(5)	692.0(5)
1.83	5.298(3)	9.183(4)	14.23(2)	90.22(7)	97.21(7)	89.95(4)	686.9(4)
3.14	5.280(2)	9.147(3)	14.15(2)	90.20(6)	97.20(6)	89.92(3)	678.1(4)
3.55	5.270(3)	9.131(4)	14.14(2)	90.24(9)	97.21(9)	89.92(4)	675.0(4)

TABLE 4. Fractional atomic coordinates and isotropic displacement parameters U_{eq}/U_{iso} (Å²) at various pressures

Site	x	y	z	U_{eq}/U_{iso}
T1	0.23108(9)	0.16723(5)	0.19144(3)	0.0069(1)
	0.2310(4)	0.1670(2)	0.1915(5)	0.0053(6)
	0.2313(4)	0.1673(2)	0.1922(7)	0.0045(7)
	0.2300(6)	0.1673(3)	0.191(1)	0.006(1)
	0.2312(6)	0.1677(3)	0.191(1)	0.006(1)
T2	0.73088(9)	0.00056(4)	0.19143(9)	0.0068(1)
	0.7311(4)	0.0005(2)	0.1931(5)	0.0060(6)
	0.7321(4)	0.0008(2)	0.1927(7)	0.0044(6)
	0.7304(7)	0.0005(3)	0.191(1)	0.007(1)
	0.7312(7)	0.0007(3)	0.191(1)	0.009(1)
M1	0	0	0	0.0069(2)
	0	0	0	0.0045(7)
	0	0	0	0.0033(8)
	0	0	0	0.005(1)
	0	0	0	0.005(1)
M2	0.0009(1)	0.33362(5)	−0.00001(3)	0.0070(2)
	0.0010(3)	0.3335(2)	−0.0010(4)	0.0044(6)
	−0.0003(3)	0.3336(2)	−0.0003(5)	0.0033(7)
	−0.0015(5)	0.3329(3)	−0.0005(7)	0.0062(9)
	−0.0003(5)	0.3331(3)	−0.0003(8)	0.0069(9)
M3	−0.0002(1)	0.16677(5)	0.50000(3)	0.0073(2)
	−0.0006(3)	0.1667(2)	0.5000(4)	0.0037(6)
	−0.0003(3)	0.1665(2)	0.5002(5)	0.0031(7)
	−0.0015(6)	0.1671(3)	0.4994(8)	0.006(1)
	−0.0005(5)	0.1671(3)	0.4995(8)	0.0048(9)
M4	0	½	½	0.0067(2)
	0	½	½	0.0031(7)
	0	½	½	0.0024(8)
	0	½	½	0.006(1)
	0	½	½	0.004(1)
O1	0.1925(2)	0.1669(1)	0.07681(8)	0.0081(2)
	0.1905(9)	0.1667(5)	0.077(1)	0.003(1)
	0.1908(9)	0.1667(5)	0.078(1)	0.004(1)
	0.192(2)	0.1661(8)	0.079(3)	0.012(3)
	0.189(2)	0.1665(9)	0.077(3)	0.020(4)
O2	0.6923(2)	0.0003(1)	0.07686(8)	0.0084(2)
	0.6935(9)	0.0005(5)	0.076(1)	0.006(1)
	0.6921(9)	0.0009(5)	0.078(1)	0.003(1)
	0.694(2)	0.0012(8)	0.080(3)	0.012(4)
	0.695(2)	0.0002(8)	0.082(3)	0.015(3)
O3	0.2141(3)	0.3339(1)	0.23258(8)	0.0157(3)
	0.2084(9)	0.3336(6)	0.233(1)	0.014(1)
	0.206(1)	0.3344(6)	0.235(1)	0.014(1)
	0.200(2)	0.3339(8)	0.238(2)	0.015(2)
	0.200(2)	0.3339(8)	0.235(2)	0.020(2)
O4	0.5102(3)	0.0994(1)	0.23276(8)	0.0156(3)
	0.5137(9)	0.1028(6)	0.234(1)	0.016(1)
	0.5148(9)	0.1042(6)	0.234(1)	0.014(1)
	0.521(1)	0.1066(8)	0.238(2)	0.018(2)
	0.522(1)	0.1071(8)	0.239(2)	0.018(2)
O5	0.0103(3)	0.0686(2)	0.23257(8)	0.0157(3)
	0.0131(9)	0.0656(6)	0.232(1)	0.016(1)
	0.0132(9)	0.0638(6)	0.236(1)	0.014(1)
	0.019(1)	0.0620(8)	0.238(2)	0.016(2)
	0.021(1)	0.0620(8)	0.240(2)	0.017(2)

TABLE 4.—*Continued*

Site	x	y	z	U_{eq}/U_{iso}
OH1	0.6913(3)	0.3335(1)	0.07334(8)	0.0098(2)
	0.6905(9)	0.3331(5)	0.077(1)	0.006(1)
	0.6921(9)	0.3331(6)	0.078(1)	0.005(1)
	0.697(1)	0.3323(7)	0.082(2)	0.006(2)
	0.700(1)	0.3327(7)	0.087(2)	0.006(2)
OH2	0.1465(3)	−0.0003(2)	0.43043(8)	0.0155(3)
	0.1450(9)	−0.0001(6)	0.427(1)	0.015(1)
	0.1475(9)	−0.0007(6)	0.426(1)	0.012(1)
	0.143(1)	−0.0014(7)	0.424(2)	0.012(2)
	0.142(1)	−0.0005(8)	0.418(2)	0.015(2)
OH3	0.1418(3)	0.3345(1)	0.43035(8)	0.0157(3)
	0.141(1)	0.3344(6)	0.428(1)	0.016(1)
	0.140(1)	0.3349(6)	0.425(1)	0.014(1)
	0.137(1)	0.3346(2)	0.422(2)	0.012(2)
	0.139(1)	0.3338(8)	0.420(2)	0.016(2)
OH4	0.6419(3)	0.1651(1)	0.43078(8)	0.0144(3)
	0.6409(9)	0.1649(6)	0.428(1)	0.012(1)
	0.6408(9)	0.1649(6)	0.426(1)	0.010(1)
	0.641(1)	0.1654(7)	0.422(2)	0.009(2)
	0.641(1)	0.1661(7)	0.421(2)	0.010(2)
H1	0.703(7)	0.337(4)	0.132(2)	0.054(6)
H2	0.122(7)	0.001(4)	0.374(2)	0.054(6)
H3	0.121(7)	0.334(4)	0.375(2)	0.054(6)
H4	0.607(8)	0.156(4)	0.377(2)	0.054(6)

Notes: For each atom values from top to bottom correspond to the refinements at 0.0001, 1.83, 3.14, 4.25, and 4.85 GPa. The H positions are those from the refinement in air. The occupancy of Mg against Fe in M sites in air refined to 0.905(3), 0.907(3), 0.936(3), and 0.938(3) Mg atoms for M1, M2, M3, and M4, respectively. The occupancy of Si against Al in T sites refined to 0.654(4) and 0.652(4) for T1 and T2, respectively. Estimated standard deviations refer to the last digit.

calibrants. Therefore in each data collection the number of reflections suitable for the structure refinement is strongly reduced. This is a significant difficulty when the symmetry of the sample is low, as in the case of triclinic chlorite. Each data collection yielded only 250–300 independent data, making the data/parameter ratio very unfavorable. The refinement was unstable, and bond lengths and angles were scattered and with large e.s.d. values, preventing reliable conclusions on the baric evolution of the structure, especially at the lower pressures. Therefore, for the refinements at 1.83 and 3.14 GPa we adopted a different strategy, collecting data with two different mountings of the sample in the DAC. A second crystal was mounted (sample 2) and further intensity data were collected at pressure values near to those of the first mounting. Due to the morphology of the samples, (0 0 1) crystal planes lie nearly parallel to the diamond culets in both mountings. However, the slightly different orientations allowed the measurement of different sets, which were corrected for the appropriate physical factors, rescaled and merged to obtain a larger set of independent data, typically consisting of about 370–400 unique reflections, with high redundancy.

The least-squares refinements with data measured at 1.83, 3.14, 4.25, and 4.85 GPa were performed with the SHELX-97 program (Sheldrick 1997). Isotropic atomic displacement parameters were used for all atoms and the site occupancies were fixed to the values resulting from the refinement in air. Details of data collections and refinements are listed in Table 1. The observed and calculated structure factors are reported in Table 3[1], fractional atomic coordinates and the displacement parameters are reported in Table 4.

RESULTS

Results of the refinement at room pressure

The structural results of the refinement are in very good agreement with literature data. In particular, the partial ordering of

for an approximate estimate of the pressure (Comodi and Zanazzi 1993); the quartz crystal was used for precise measurement of the pressure (Angel et al. 1997). The uncertainties in the pressure calibration based on the equation of state of quartz were estimated to be less than 0.05 GPa. The experiments were carried out in the pressure range 10^{-4}–5.5 GPa. Higher pressure was hindered by failure of the gasket. The crystal was recovered and examined in air at room conditions: the sample showed severe signs of damage, with streaked reflections and lower intensities.

The DAC was centered on the diffractometer following the procedure of Budzianowski and Katrusiak (2004). Intensity data were collected with the CCD detector, then corrected for absorption using Absorb V6.0 software (Angel 2004). After each intensity data collection, the unit-cell parameters of chlorite and quartz were accurately measured with the point detector. Several reflections between 40 and 80 in the θ range 5–28° were used.

The diffracted intensities from the sample in the DAC are few and of poor quality because of the blind zones due to instrumental limits and the occasional overlapping positions with other phases present in the cell, namely the two diamonds, the powder rings of the beryllium disks, the Sm^{2+}:BaClF and quartz used as pressure

[1] Deposit item AM-06-032, Table 3, observed and calculated structure factors. Deposit items are available two ways: For a paper copy contact the Business Office of the Mineralogical Society of America (see inside front cover of recent issue) for price information. For an electronic copy visit the MSA web site at http://www.minsocam.org, go to the American Mineralogist Contents, find the table of contents for the specific volume/issue wanted, and then click on the deposit link there.

trivalent cations in the brucite-type layer with preference for the M4 site, as suggested for triclinic chlorites by Joswig and Fuess (1990) and Joswig et al. (1980), is confirmed. M4-O mean bond length is 2.021 Å, while M3-O is 2.041 Å, and M1-O and M2-O are 2.079 and 2.079 Å, respectively. The Si and Al in tetrahedra are disordered, T1-O and T2-O mean bond lengths being 1.650 Å, with equal Si/Al occupancy. The tetrahedral rotation angle α, defined as the difference between 120° and the Φ angles formed by the basal O-O edges of adjacent tetrahedra [$2\alpha = \Sigma_{i=1,6}(|120 - \Phi_i|)/6$, Weiss et al. 1992], is 6.1°. The three OH groups of the brucite-type layer are involved as donors in H-bonds with the basal O atoms of the tetrahedral sheet. The O-O distances are 2.919, 2.918, and 2.908 Å, respectively for the OH2-O5, OH3-O3, and OH4-O4 interactions. Table 5 lists bond distances and geometrical parameters.

Compressibility

The unit-cell parameters at various pressures are listed in Table 2 and shown in Figure 1. A third-order Birch-Murnaghan Equation of State (EoS) is the best approximation to describe the chlorite volume evolution with P, as suggested by plotting the "normalized stress" vs. the Eulerian finite strain (Jeanloz and Hazen 1991; Angel 2000, 2001) (Fig. 2). The refined EoS parameters are $V_0 = 701.8(1)$ Å³, very close to the measured value (Table 2), $K_0 = 88(5)$ GPa and $K' = 5(3)$. Weighted χ^2 is 4.4, maximum ΔP is 0.2 GPa. The value of bulk modulus obtained by fitting data with a 2nd-order EoS (K' fixed to 4) is 89(3) GPa.

Compressibility data for chlorite in literature are quite scattered. Excluding the Hazen and Finger (1978) value (55 GPa) for the reasons already described, the bulk moduli determined from both natural and synthetic chlorite are $K_0 = 69(1)$ GPa (synthetic chamosite, EDS synchrotron data, Theye et al. 2003); 75.4(2.7) GPa (synthetic clinochlore, neutron powder-diffraction, Welch and Marshall 2001); 77.6(1.1) GPa (synthetic clinochlore, Grevel et al. 1997); 78.6(1.2) GPa (natural clinochlore, Theye et al. 2003); 81.0(5) GPa (synthetic clinochlore, synchrotron powder-diffraction data, Welch and Crichton 2002); 83.4(7) GPa for Mg-chlorite, 89.5(27) GPa for synthetic clinochlore, 84.1(8) GPa for Fe-chlorite (EDS synchrotron data, Pawley et al. 2002); 91.1(3.9) GPa (natural chamosite, Theye et al. 2003). All these values were obtained for second order fits ($K' = 4$) and constraining the lattice to monoclinic symmetry, or occasionally to hexagonal symmetry (Theye et al. 2003). The data of Welch and Crichton (2002) and Pawley et al. (2002) show the better agreement with our data (difference less than 1.2%). Main differences between our data and those in literature may arise from the different methodologies employed, single-crystal vs. powder diffraction, and the nature of the samples. In any case, the value of bulk modulus of 47.2 GPa in the databases of Berman (1988) and Holland and Powell (1998) should be revised.

Chlorite is stiffer than other layer structures, when its bulk modulus is compared to those of other phyllosilicates such as talc (41.6 GPa, Pawley et al. 1995) and micas [54 GPa in phlogopite, Comodi et al. 2004; in the range 52–61 GPa in 2M$_1$ muscovites, 58–62 GPa in 2M$_1$ and 3T phengites, 66 GPa in paragonite, see Table 1 in Zanazzi and Pavese (2002) and references therein], or with brucite (47 GPa, Parise et al. 1994; 41 GPa, Catti et al. 1995; 44 GPa, Nagai et al. 2000).

TABLE 5. Values of bond distances (Å), polyhedral volumes (Å³), and distortion parameters (following Robinson et al. 1971) at various pressures

P (GPa)	0.0001	1.83	3.14	4.25	4.85
T1-O1	1.636(1)	1.62(2)	1.60(2)	1.57(3)	1.58(4)
-O3	1.653(1)	1.650(8)	1.65(1)	1.67(1)	1.65(1)
-O4	1.654(2)	1.653(6)	1.643(8)	1.68(1)	1.69(1)
-O5	1.656(1)	1.65(1)	1.67(1)	1.67(1)	1.68(2)
<T1-O>	1.650	1.64	1.64	1.65	1.65
V_{T1}	2.30(1)	2.27(5)	2.26(5)	2.28(8)	2.30(9)
σ^2T1 *	2.38	3.06	3.99	17.11	20.80
λ_{T1} †	1.001	1.001	1.001	1.004	1.005
T2-O2	1.635(1)	1.65(2)	1.60(2)	1.56(3)	1.52(4)
-O4	1.654(2)	1.647(9)	1.65(1)	1.66(2)	1.67(1)
-O5	1.655(1)	1.640(5)	1.636(7)	1.67(1)	1.68(1)
-O3	1.657(1)	1.65(1)	1.65(1)	1.68(2)	1.66(2)
<T2-O>	1.650	1.65	1.63	1.64	1.63
V_{T2}	2.30(1)	2.29(5)	2.24(5)	2.22(6)	2.22(8)
σ^2_{T2} *	2.43	0.99	3.63	18.82	17.66
λ_{T2} †	1.001	1.000	1.001	1.004	1.005
Tetr. rot. α §	6.1(1)	7.3(4)	7.8(5)	9.0(5)	9.1(3)
T sheet thickness	2.223(2)	2.21(1)	2.20(1)	2.22(2)	2.21(3)
M1-OH1×2	2.062(1)	2.074(8)	2.08(1)	2.11(1)	2.15(2)
-O1×2	2.086(1)	2.066(7)	2.07(1)	2.07(2)	2.05(2)
-O2×2	2.089(1)	2.06(1)	2.08(1)	2.07(2)	2.10(2)
<M1-O>	2.079	2.07	2.07	2.08	2.10
V_{M1}	11.81(2)	11.6(1)	11.8(1)	12.0(2)	12.2(3)
ψ_{M1} ‡	58.7	58.4	58.0	57.4	56.7
σ^2_{M1} *	33.00	28.56	22.14	14.67	8.72
λ_{M1} †	1.010	1.009	1.007	1.004	1.003
M2-OH1	2.064(1)	2.063(8)	2.07(1)	2.09(1)	2.13(2)
-OH1	2.067(1)	2.10(1)	2.08(1)	2.09(1)	2.12(2)
-O2	2.082(1)	2.075(8)	2.08(1)	2.09(2)	2.10(2)
-O2	2.088(1)	2.064(9)	2.07(1)	2.07(2)	2.10(2)
-O1	2.084(1)	2.07(1)	2.08(1)	2.08(2)	2.07(2)
-O1	2.088(1)	2.076(9)	2.08(1)	2.08(2)	2.05(2)
<M2-O>	2.079	2.07	2.07	2.08	2.10
V_{M2}	11.80(2)	11.7(1)	11.8(1)	12.0(2)	12.2(3)
ψ_{M2} ‡	58.7	58.6	58	57.4	56.7
σ^2_{M2} *	33.01	30.40	22.19	14.76	9.86
λ_{M2} †	1.010	1.009	1.007	1.004	1.003
O sheet thickness	2.159(4)	2.16(2)	2.20(2)	2.25(3)	2.30(2)
M3-OH4	2.036(2)	2.04(1)	2.05(1)	2.07(2)	2.07(2)
-OH4	2.037(2)	2.044(7)	2.05(1)	2.05(1)	2.06(2)
-OH3	2.042(2)	2.046(8)	2.06(1)	2.09(2)	2.09(2)
-OH3	2.044(1)	2.05(1)	2.07(1)	2.06(2)	2.08(2)
-OH2	2.043(2)	2.05(1)	2.06(1)	2.07(2)	2.10(2)
-OH2	2.044(1)	2.05(1)	2.06(1)	2.06(2)	2.10(2)
<M3-O>	2.041	2.05	2.06	2.07	2.08
V_{M3}	10.93(2)	11.1(1)	11.4(1)	11.6(2)	12.0(3)
ψ_{M3} ‡	60.9	60.1	59.4	58.4	57.4
σ^2_{M3} *	77.2	57.54	44.80	28.36	15.29
λ_{M3} †	1.025	1.018	1.014	1.009	1.005
M4-OH2×2	2.018(1)	2.030(7)	2.02(1)	2.04(1)	2.08(2)
-OH4×2	2.022(1)	2.03(1)	2.03(1)	2.06(2)	2.07(2)
-OH3×2	2.022(1)	2.03(1)	2.04(1)	2.05(2)	2.07(2)
<M4-O>	2.021	2.03	2.03	2.05	2.07
V_{M4}	10.65(2)	10.9(1)	11.0(1)	11.4(2)	11.8(3)
ψ_{M4} ‡	60.6	59.7	58.9	58.1	57.3
Σ^2_{M4} *	69.6	51.05	36.39	24.21	13.55
λ_{M4} †	1.022	1.016	1.011	1.007	1.004
O sheet thickness	1.983(5)	2.04(2)	2.10(1)	2.17(3)	2.24(2)
OH2-O5	2.919(2)	2.85(2)	2.76(3)	2.69(4)	2.58(4)
OH3-O3	2.918(2)	2.83(2)	2.75(2)	2.65(4)	2.66(4)
OH4-O4	2.908(2)	2.81(2)	2.77(2)	2.65(4)	2.62(4)
TOT···O thickness	2.824(3)	2.75(2)	2.68(3)	2.58(4)	2.54(5)
TOT thickness	6.605(3)	6.58(3)	6.59(2)	6.69(5)	6.73(5)

Notes: Estimated standard deviations refer to the last digit.
* σ^2 is the angle variance (deg²).
† λ is the quadratic elongation.
‡ Ψ is the octahedral flattening angle (deg); see text for definition.
§ α is the tetrahedral rotation angle (deg); see text for definition.

The "axial moduli" were obtained by fitting a 2nd-order Birch-Murnaghan EoS for the a and b axes and a 3rd-order Birch-Murnaghan EoS for the c axis, giving $a_0 = 5.332(1)$ Å, $K_0 = 99(2)$
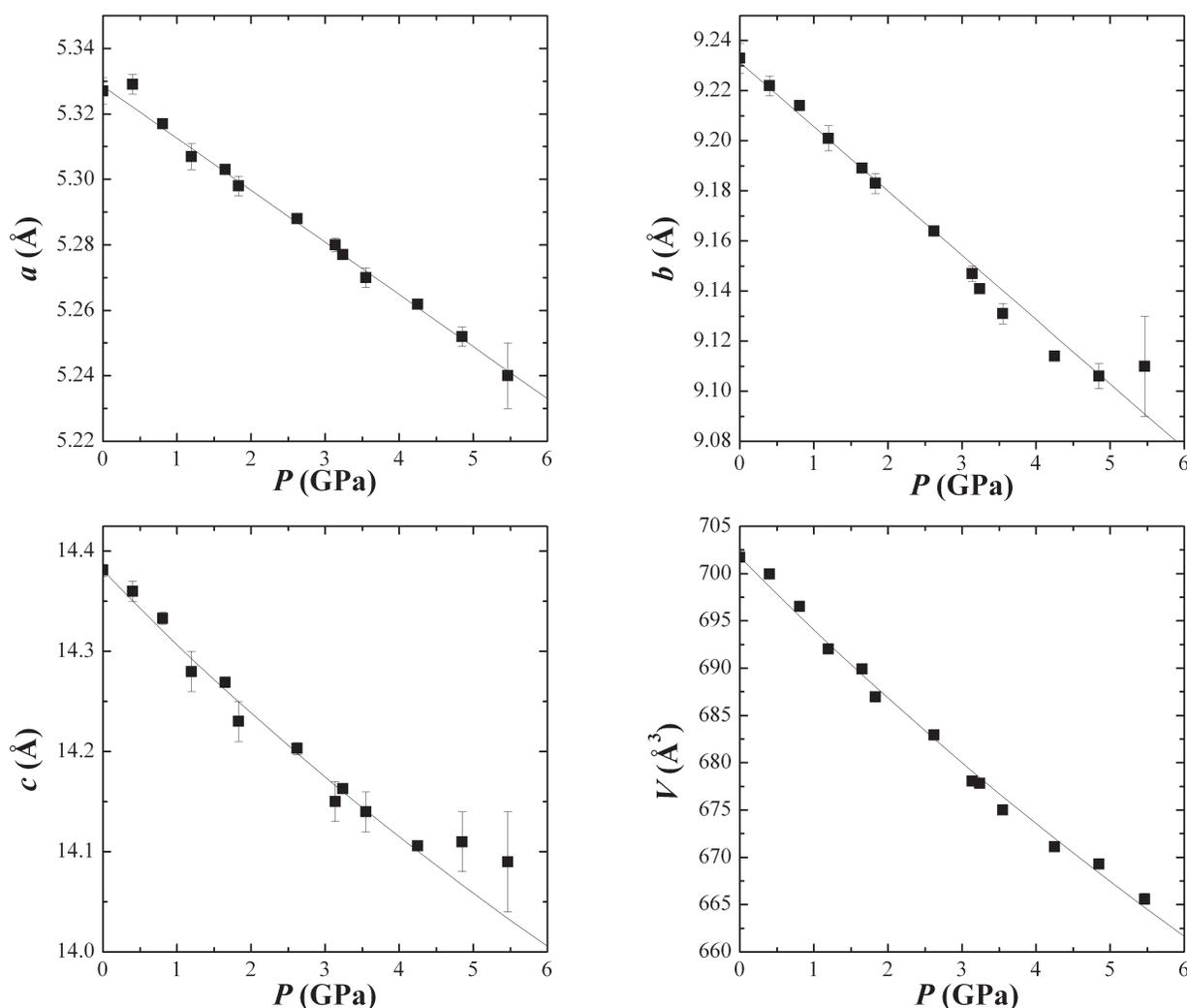
FIGURE 1. Variations of unit-cell parameters of chlorite as a function of pressure. Solid curves represent the Birch-Murnaghan EoS best fit.

GPa; $b_0 = 9.239(2)$ Å, $K_0 = 97(2)$ GPa; $c_0 = 14.387(6)$ Å, $K_0 = 62(7)$ GPa, and $K' = 5(3)$ values. The axial compressibility values (inverse of axial moduli divided by three), were $\beta_{0a}^{EoS} = 3.4(2)$, $\beta_{0b}^{EoS} = 3.4(1)$, and $\beta_{0c}^{EoS} = 5.4(2)$ 10^{-3} GPa^{-1}. The chlorite behavior is not unlike other phyllosilicates and micas, in that the c axis is most affected by pressure, due to the layered nature of these phases. Along the [0 0 1] direction chlorite is about 2 and 2.5 times less compressible than talc and phlogopite; micas shows the highest β_{0c}^{EoS} (13.3 10^{-3} GPa^{-1}, Comodi et al. 2004). However, chlorite has a greater compressibility in the a-b plane, with respect to other layer silicates; i.e., in phlogopite the axial compressibilities along a and b are 2.7 and 2.6 10^{-3} GPa^{-1}. Therefore the chlorite structure behaves anisotropically with pressure, but to a lesser extent than other layer silicates.

The lattice retains triclinic symmetry over the studied pressure range. The cell angle γ does not vary significantly, α slightly decreases, whereas β slightly increases (Fig. 3). A similar behavior was observed in phlogopite (Comodi et al. 2004) and talc in experimental (Pawley et al. 1995) and theoretical (Stixrude 2002) studies.

STRUCTURAL EVOLUTION WITH P

The stacking sequence of chlorite is characterized by 2:1 talc- and brucite-type layers, each contributing in a different way to the structural behavior at pressure. Table 5 lists the bond distances, as well as some geometrical parameters. We analyze how each chlorite polyhedron of the different layers is modified with increasing pressure. The octahedra of both talc- and brucite-type layers tilt and become more regular with pressure, as shown by the angle variance values (Robinson et al. 1971) reported in Table 5. Moreover, pressure dependence of the ψ angle (the angle between the body diagonal of the octahedron and the vertical, Bailey 1988), shows that the flattening of the octahedra decreases with P (Fig. 4), leading to a regularization and to an increase in the volume of the octahedron. As a consequence, a thickening along c^* and a reduction in the a-b plane of the octahedral sheet is achieved; the same mechanism was also observed in brucite (Parise et al. 1994; Nagai et al. 2000). On the contrary, tetrahedra distortion increases with P (Fig. 5), the tetrahedral thickness remains almost unchanged and the tetrahedral volumes slightly
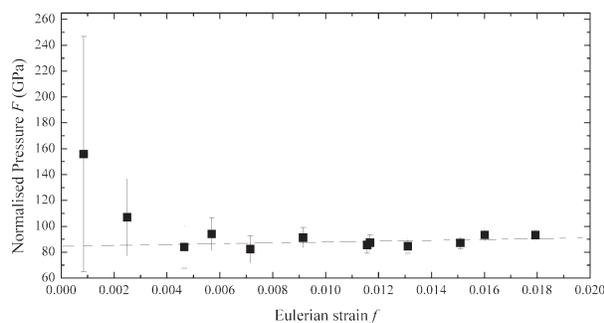
FIGURE 2. Plot of the "normalized stress" defined as $F_E = P/[3f_E(1 + 2f_E)^{5/2}]$, vs. the finite strain $f_E = [(V_0/V)^{2/3} - 1]/2$. The first two points were excluded from the fit. Chlorite volume data are adequately described by a 3rd-order truncation of the EoS.
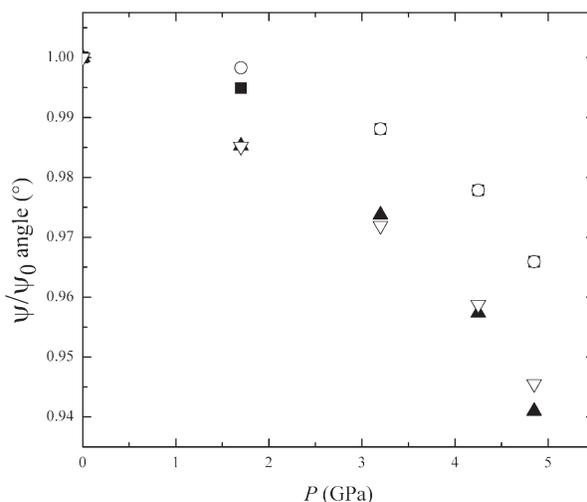

FIGURE 4. Flattening of the octahedra (Ψ, see text for definition) with pressure; solid squares, open circles, solid up-triangles, and open down-triangles refer to M1, M2, M3, and M4 octahedra, respectively. Values are normalized to the room pressure data.

FIGURE 3. Variations of the unit-cell angles with pressure. Solid squares, solid circles and open squares refer to α, β, and γ cell angles, respectively.
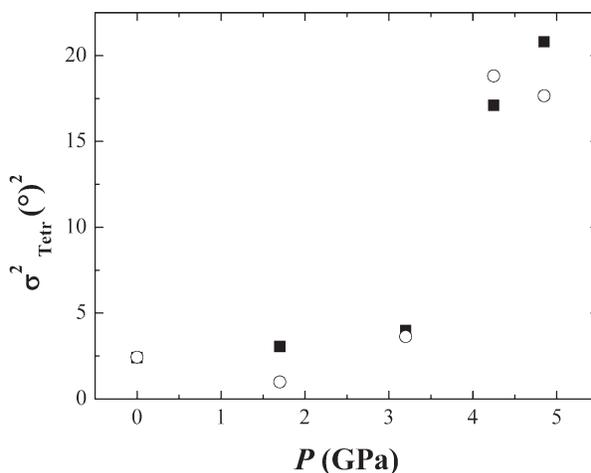
FIGURE 5. Tetrahedral angle variance (Robinson et al. 1971) in the investigated pressure range; solid squares and open circles refer to T1 and T2 tetrahedra, respectively.

decrease (Table 5). The tetrahedral distortion at high pressure could be also ascribed to the increased hydrogen bond strength between the OH of the brucite-type layer and the basal O of the tetrahedral sheet (Fig. 6).

On the whole, the polyhedral distortion with P can explain the apparent anomalous result observed in the evolution of the volume of octahedra and tetrahedra: the volume slightly increases in the former and decreases in the latter, according to the general rule that regular polyhedra have the maximum volume with respect to any distorted polyhedra.

As in all layer silicates, to achieve dimensional matching of the relatively incompressible tetrahedral sheet with the more laterally compressible octahedral sheet, an increase of the ditrigonalization α of the six-member tetrahedral rings is required. In chlorite, α increases with pressure from 6.1 to 9.1° and this ditrigonalization reflects both the requirement for TOT misfit and the strengthening of OH-O hydrogen bonds, due to the thinning of the interlayer and the shortening of the O-O distances with

P (Figs. 6 and 7).

The interlayer region faces the talc-type to the brucite-type layer; here the hydrogen bonds formed between the layers affect the structural properties of the phase. In fact, in the studied pressure range the thickness of the brucite-type sheet increases by 11.5% whereas the T-O-T thickness increases by only 1.8%. On the contrary the interlayer is reduced of about 10%, and despite the increase in the thickness of brucite- and talc-type sheets, the greatest contraction of the structure is achieved normal to the sheets. Between 3.2 and 4.25 GPa the OH-O distance approaches the value of 2.7 Å, limit below which the O^{2-}-O^{2-} are considered to be in contact (Brown 1976). Welch et al. (2004) suggested for clinochlore that this contact distance could be reached at about 8 GPa and after this pressure an anomalous structural behavior may occur. At 4.85 GPa however we found shorter O⋯O dis-
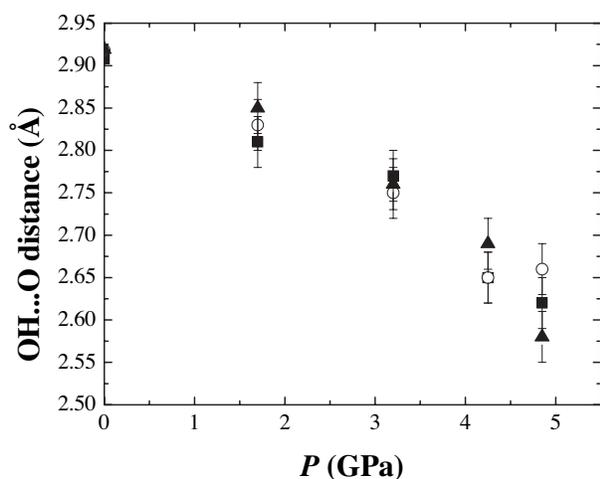
FIGURE 6. The interlayer OH···O distances vs. pressure; solid squares, open circles, and solid up-triangles refer to OH4-O4, OH3-O3, and OH2-O5 H-bonds, respectively.

tances, in the range 2.66–2.58 Å (Fig. 6), without significant structure variations. When the 2.7 Å contact limit is reached, the main effect we find is the enhancement of the polyhedra distortion parameters, i.e., the tetrahedral angle variance (Fig. 5). Spectroscopic study by Kleppe et al. (2003) showed a strong discontinuity with a large increase in dv/dP for the OH mode of the brucite-type layer at 9–10 GPa. The high positive shifts of the O-H mode with P have been related by Hofmeister et al. (1999) to a H-H cation repulsion, which is a consequence of the decrease of the OH-O angle. Neutron diffraction data for clinochlore showed a considerable decrease in the OH-O angle from 170 to 155° (Welch and Marshall 2001), which is consistent with the in-plane movement of basal oxygen by an O-rotation of the tetrahedral ring (Fig. 7). The peculiar stiffer character of chlorite can be mainly ascribed to the narrower interlayer space due to non-superimposed cations across the interlayer. At high P, the repulsive effects between OH and O caused by the interlayer shortening could explain the smaller compressibility along the c axis relative to other layer silicates, as well as the anisotropy in the cell deformation.

DISCUSSION AND CONCLUSION

To a first approximation, considering the structural effects of P and T to be approximately inversely related, we use our experimentally determined compressibility and thermal expansion from literature to define a P-V-T EoS. Pawley et al. (2002) suggested that the chemical substitutions in chlorite do not affect significantly the compressibility, in contrast to that observed for thermal behavior, which is strongly influenced by the Fe/Mg content (Symmes 1986). Nelson and Guggenheim (1993) obtained a thermal expansion coefficient for a chlorite having a composition quite similar to that of our sample. We combine this coefficient with our compressibility data to obtain the equation: $V = V_0(1 - 1.14\ 10^{-2}\ \Delta P + 2.316\ 10^{-5}\ \Delta T)$, where P is in GPa and T is in Celsius.

Using the EoS obtained in this study, we compute the thermal gradient for which the cell volume of chlorite is invariant. As-
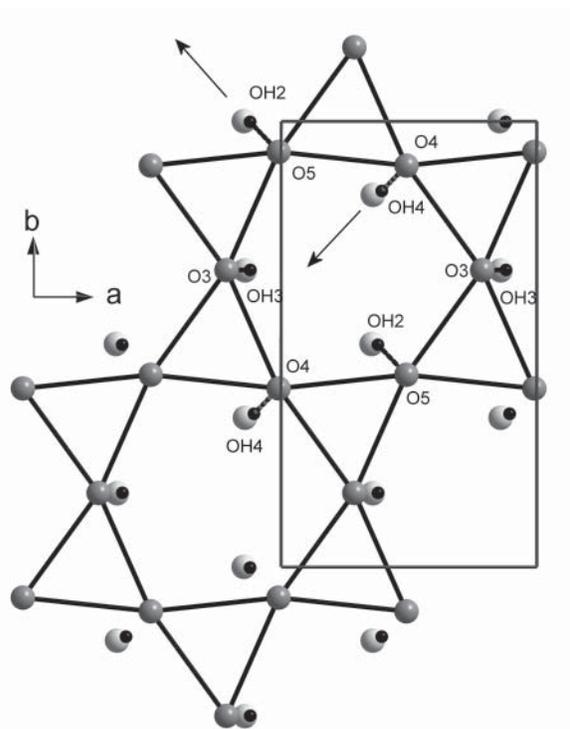
FIGURE 7. View of the chlorite interlayer along [001]. Basal O atoms (dark gray) of the T sheet are superimposed on the hydroxyls (light gray oxygen and black dot hydrogen) of the OH-layer of the brucite-type sheet. The dashed arrows indicate the sense of movement induced by pressure: the greater OH2-O5 and OH4-O4 bond strengths (shorter OH2-O5 and OH4-O4 distances) yield the decrease of the O3-O5-O4 angle, and the increase of the O5-O4-O3 angle, explaining the enhancement in ditrigonalization of the sixfold basal ring.

suming an average rock density of 2.7 g/cm^3, the isochoric P-T path will correspond to a geothermal gradient of 18 °C/km, a value similar to that calculated for serpentine (20 °C/km, Mellini 2000). This gradient is compatible with a geotherm along an early subduction and slow convergence slab (Kincaid and Sacks 1997).

Since chlorite is involved in several phase-equilibrium reactions (i.e., with antigorite, amphibole, enstatite, 10 Å phase) an accurate evaluation of the bulk modulus is important in defining its behavior at HP. Its bulk modulus is higher than the other layer silicates, possibly because of the peculiar topology of the interlayer, where the OH-bonding system between the brucite- and talc-type layers makes the chlorite structure stiffer. The value of 88 GPa measured in this work is significantly different from the value 49.7 GPa reported in current databases (e.g., Holland and Powell 1998). The discussion of petrological phase equilibria is beyond the scope of this paper, but care should be taken when thermodynamic stability calculations are performed using current databases.

ACKNOWLEDGMENTS

REFERENCES CITED

Angel, R.J. (2000) Equation of State. In R.M. Hazen and R.T. Downs, Eds., High-Temperature and High-Pressure Crystal Chemistry, 41, p. 35–59. Reviews in Mineralogy and Geochemistry, Mineralogical Society of America, Chantilly, Virginia.

——— (2001) EOS-FIT V6.0. Computer program. Crystallography Laboratory, Department Geological Sciences, Virginia Polytechnic Institute and State University, Blacksburg.

——— (2004) Program for absorption. Crystallography Laboratory, Department Geological Sciences, Virginia Polytechnic Institute and State University, Blacksburg.

Angel, R.J., Allan, D.R., Miletich, R., and Finger, L.W. (1997) The use of quartz as an internal pressure standard in high-pressure crystallography. Journal of Applied Crystallography, 30, 461–466.

Bailey, S.W. (1988) Chlorites: structures and crystal chemistry. In S.W. Bailey, Ed., Hydrous Phyllosilicates (exclusive of micas), 19, p. 347–403. Reviews in Mineralogy, Mineralogical Society of America, Chantilly, Virginia.

Bayliss, P. (1975) Nomenclature of the trioctahedral chlorites. Canadian Mineralogist, 13, 178–180.

Berman, R.G. (1988) Internally consistent thermodynamic data for minerals in the system $Na_2O\text{-}K_2O\text{-}CaO\text{-}MgO\text{-}FeO\text{-}Fe_2O_3\text{-}Al_2O_3\text{-}SiO_2\text{-}TiO_2\text{-}H_2O\text{-}CO_2$. Journal of Petrology, 29, 445–552.

Brown, I.D. (1976) On the Geometry of O-H···O Hydrogen Bonds. Acta Crystallographica, A32, 24–31.

Budzianowski, A. and Katrusiak, A. (2004) High-pressure crystallographic experiments with a CCD-detector. In A. Katrusiak and P. McMillan, Eds., High-Pressure Crystallography, p. 101–112. Kluver Academic Publishers, The Netherlands.

Catti, M., Ferraris, G., Hull, S., and Pavese, A. (1995) Static compression and H disorder in brucite, $Mg(OH)_2$, to 11 GPa: a powder neutron diffraction study. Physics and Chemistry of Minerals, 22, 200–206.

Comodi, P. and Zanazzi, P.F. (1993) Improved calibration curve for the Sm^{2+}: BaFCl pressure sensor. Journal of Applied Crystallography, 26, 843–845.

Comodi, P., Fumagalli, P., Montagnoli, M., and Zanazzi, P.F. (2004) A single-crystal study on the pressure behavior of phlogopite and petrological implications. American Mineralogist, 89, 647–653.

Fumagalli, P. and Poli, S. (2005) Experimentally determined phase relations in hydrous peridotites to 6.5 GPa and their consequences on the dynamics of subduction zones. Journal of Petrology, 46, 555–578.

Grevel, K., Fasshauer, D.W., and Erzner, S. (1997) New compressibility data for clinochlore, kyanite, Mg-chloritoid, and Mg-staurolite. European Journal of Mineralogy, 1, 138.

Hazen, R.M. and Finger, L.W. (1978) The crystal structures and compressibilities of layer minerals at high pressure. II. Phlogopite and chlorite. American Mineralogist, 63, 293–296.

Hofmeister, A.M., Cynn, H., Burnley, P.C., and Meade, C. (1999) Vibrational spectra of dense, hydrous magnesium silicates at high pressure: Importance of hydrogen bond angle. American Mineralogist, 84, 454–464.

Holland, T.J.B. and Powell, R. (1998) An internally consistent thermodynamic data set for phases of petrological interest. Journal of Metamorphic Geology, 16, 309–343.

Jeanloz, R. and Hazen, R.M. (1991) Finite-strain analysis of relative compressibilities. Application to the high-pressure wadsleyite phase as an illustration. American Mineralogist, 76, 1765–1768.

Joswig, W. and Fuess, H. (1989) Neutron diffraction study of a one-layer monoclinic chlorite. Clays and Clay Minerals, 37, 511–514.

——— (1990) Refinement of a one-layer triclinic chlorite. Clays and Clay Minerals, 38, 216–218.

Joswig, W., Fuess, H., Rothbauer, R., Takeuchi, Y., and Mason, S.A. (1980) A neutron diffraction study of a one-layer triclinic chlorite (penninite). American Mineralogist, 65, 349–352.

Kincaid, C. and Sacks, I.S. (1997) Thermal and dynamical evolution of the upper mantle in subduction zones. Journal of Geophysical Research, 102, 12295–12315.

Kleppe, A.K., Jephcoat, A.P., and Welch, M.D. (2003) The effect of pressure upon hydrogen bonding in chlorite: a Raman spectroscopic study of clinochlore to 26.5 GPa. American Mineralogist, 88, 567–573.

Mellini, M. (2000) Mineral Behaviour across the Crust-Mantle Boundary. In G. Ranalli, C.A. Ricci, and V. Trommsdorff, Eds., Proceedings of the International School Earth and Planetary Sciences, "Crust-Mantle Interactions," Siena, 2000, 65–76.

Nagai, T., Hattori, T., and Yamanaka, T. (2000) Compression mechanism of brucite: An investigation by structural refinement under pressure. American Mineralogist, 85, 760–764.

Nelson, D.O. and Guggenheim, S. (1993) Inferred limitations to the oxidation of Fe in chlorite: A high-temperature single-crystal X-ray study. American Mineralogist, 78, 1197–1207.

Parise, J.B., Leinenweber, K., Weidner, D.J., Tan, K., and Von Dreele, R.B. (1994) Pressure-induced H bonding: Neutron diffraction study of brucite, $Mg(OD)_2$, to 9.3 GPa. American Mineralogist, 79, 193–196.

Pawley, A. (2003) Chlorite stability in mantle peridotites: reaction clinochlore + enstatite = forsterite + pyrope + H_2O. Contributions to Mineralogy and Petrology, 144, 449–456.

Pawley, A.R., Redfern, S.A.T., and Wood, B.J. (1995) Thermal expansivities and compressivities of hydrous phases in the system $MgO\text{-}SiO_2\text{-}H_2O$: talc, phase A, and 10 Å phase. Contributions to Mineralogy and Petrology, 122, 301–307.

Pawley, A.R., Clark, S.M., and Chinnery, N.J. (2002) Equation of state measurements of chlorite, pyrophyllite, and talc. American Mineralogist, 87, 1172–1182.

Phillips, T.L., Loveless, J.K., and Bailey, S.W. (1980) Cr^{3+} coordination in chlorites: A structural study of ten chromian chlorites. American Mineralogist, 65, 112–122.

Poli, S. and Schmidt, M.W. (2002) Petrology of subducted slabs. Annual Review of Earth and Planetary Sciences, 30, 207–235.

Robinson, K., Gibbs, G.V., and Ribbe, P.H. (1971) Quadratic elongation, a quantitative measure of distortion in coordination polyhedra. Science, 172, 191–193.

Rule, A.C. and Bailey, S.W. (1987) Refinement of the crystal structure of a monoclinic ferroan clinochlore. Clays and Clay Minerals, 35, 129–138.

Sheldrick, G.M. (1996) SADABS. Program for empirical absorption correction of area detector data. Institut für Anorganische Chemie, University of Göttingen, Germany

——— (1997) SHELX-97. Programs for crystal structure determination and refinement. Institut für Anorganische Chemie, University of Göttingen, Germany.

Steinfink, H. (1958) The crystal structure of chlorite. II. A triclinic polymorph. Acta Crystallographica, 11, 195–198.

Stixrude, L. (2002) Talc under tension and compression: Spinodal instability, elasticity, and structure. Journal of Geophysical Research, 107, 2327–2336.

Symmes, G.H. (1986) The thermal expansion of natural muscovite, paragonite, margarite, pyrophyllite, phlogopite, and two chlorites: the significance of high T/P volume studies on calculatred phase equilibria. B.A. thesis, Amherst College, Massachusetts.

Theye, T., Parra, T., and Lathe, C. (2003) Room-temperature compressibility of clinochlore and chamosite. European Journal of Mineralogy, 15, 465–468.

Ulmer, P. and Trommsdorff, V. (1995) Serpentine stability to mantle depths and subduction-related magmatism. Science, 268, 858–861.

Weiss, Z., Rieder, M., and Chmielovà, M. (1992) Deformation of coordination polyhedra and their sheets in phyllosilicates. European Journal of Mineralogy, 4, 665–682.

Welch, M.D. and Crichton, W.A. (2002) Compressibility of clinochlore to 8 GPa at 298 K and a comparison with micas. European Journal of Mineralogy, 14, 561–565.

Welch, M.D. and Marshall, W.G. (2001) High-pressure behavior of clinochlore. American Mineralogist, 86, 1380–1386.

Welch, M.D., Kleppe, A.K., and Jephcoat, A.P. (2004) Novel high-pressure behavior in chlorite: A synchrotron XRD study of clinochlore to 27 GPa. American Mineralogist, 89, 1337–1340.

Wilson, A.J.C. and Prince, E., Eds. (1999) International Tables for X-ray Crystallography, Volume C: Mathematical, physical and chemical tables (2nd edition). Kluwer Academic, Dordrecht.

Zanazzi, P.F. and Pavese, A. (2002) Behavior of micas at high pressure and high temperature. In A. Mottana, F.P. Sassi, J.B. Thompson, Jr., and S. Guggenheim, Eds., Micas: Crystal Chemistry and Metamorphic Petrology, 46, p. 99–116. Reviews in Mineralogy and Geochemistry, Mineralogical Society of America, Chantilly, Virginia.

Zheng, H. and Bailey, S.W. (1989) Structures of intergrown triclinic and monoclinic IIb chlorites from Kenya. Clays and Clay Minerals, 37, 308–316.